frontiers in Astronomy and Space Sciences

ORIGINAL RESEARCH
published: 25 March 2022
doi: 10.3389/fspas.2022.846395

Pseudo-Maxwellian Velocity Distribution Formed by the Pickup-like Process in Magnetic Reconnection

Shunsuke Usami[1,2]* *and Ritoku Horiuchi*[1]

[1]National Institute for Fusion Science, National Institutes of Natural Sciences, Toki, Japan, [2]The University of Tokyo, Tokyo, Japan

Focusing on ring-shaped ion velocity distributions with a finite width formed in magnetic reconnection in the presence of a guide magnetic field, intriguing properties such as the formation mechanism, a significant change in the shape, and necessary conditions for the change are investigated by means of theory and simulations. The width of a ring velocity distribution predominantly originates from velocity variations of seed particles for the pickup-like process. A function exactly representing a ring with a width is analytically formulated, assuming a steady supply of seed particles satisfying a Maxwellian velocity distribution and a mixing of gyration phases. The formulated function indicates that when the ring width is larger than a criterion, the local minimum of the ring's center is changed into the maximum, and the shape is transformed into a mountain shape. Such a mountain-like distribution is defined as "a pseudo-Maxwellian distribution," because it is almost indistinguishable in shape from a genuine Maxwellian distribution. Actually, particle simulations demonstrate that mountain-shaped ion velocity distributions are formed during magnetic reconnection with a guide magnetic field, and it is nearly concluded that they are pseudo-Maxwellian distributions. Moreover, two types of evidence for pseudo-Maxwellian distributions are shown by simulations. One is to analyze the dependence of the distribution shape on the guide magnetic field, which is explored by the particle simulation. In cases of slightly different values of the guide field, vague shapes of rings with a width are observed as ion velocity distributions. The other is to observe velocity distributions under a hypothetical condition of an artificial zero temperature in the upstream by utilizing a test particle simulation. In the test particle simulation, ring-shaped distributions with a width are clearly seen, because the velocity variations in the upstream are reduced. From the two types of evidence, it is definitely confirmed that the mountain-shaped distributions found in the particle simulations are pseudo-Maxwellian distribution. These results imply that pseudo-Maxwellian distributions would be created for various cases of guide field magnetic reconnection.

Keywords: ring-shaped distribution, pseudo-Maxwellian distribution, magnetic reconnection, pickup, particle simulation, test particle simulation

OPEN ACCESS

Edited by:
Fulvia Pucci,
NASA Jet Propulsion Laboratory (JPL), United States

Reviewed by:
Ruilong Guo,
Shandong University, China
Juergen Dreher,
Ruhr-University Bochum, Germany

***Correspondence:**
Shunsuke Usami
usami.shunsuke@nifs.ac.jp

Specialty section:
This article was submitted to Plasma Physics, a section of the journal Frontiers in Astronomy and Space Sciences

Received: *31 December 2021*
Accepted: *22 February 2022*
Published: *25 March 2022*

Citation:
Usami S and Horiuchi R (2022) Pseudo-Maxwellian Velocity Distribution Formed by the Pickup-like Process in Magnetic Reconnection. Front. Astron. Space Sci. 9:846395. doi: 10.3389/fspas.2022.846395

1 INTRODUCTION

Magnetic reconnection is a fundamental process in a plasma through which stored magnetic energy is rapidly released to plasma kinetic and thermal energies (Yamada, 2007). Magnetic reconnection is thought to be involved with various active phenomena in astrophysical and laboratory plasmas (Yamada et al., 2014; Burch et al., 2016) such as solar flares, substorms in the geomagnetosphere, and tokamak disruptions, and it is utilized as one of the initial heating methods in spherical tokamaks (Tanabe et al., 2017; Inomoto et al., 2019; Ono et al., 2019; Tanabe et al., 2021). In addition, magnetic reconnection has attracted the extensive attention and has been explored by many researchers for long periods of history, mainly because it contains a wide variety of research topics, such as topology change on global scale, acceleration, heating, and chaotic motions (Zenitani et al., 2017; Yoon and Bellan, 2021). In order to investigate physical processes associated with magnetic reconnection, particle velocity distributions are analyzed in many cases of satellite observations and simulation studies (Ishizawa and Horiuchi, 2005; Cheng et al., 2015; Bessho et al., 2016; Burch et al., 2016; Zenitani and Nagai, 2016; Zenitani et al., 2017; Hesse et al., 2018; Pucci et al., 2018; Horiuchi et al., 2019). In plasma physics, in particular, in cases of collisionless plasmas, velocity distributions have large amounts of information to enable us to grasp the mechanism of energy conversion and kinetic effects containing individual particle behaviors. It can be said that velocity distributions play a remarkable role in bridging macroscopic dynamics and individual particle motions.

The analysis of velocity distributions is utilized as a powerful tool, in particular, to elucidate the mechanism of plasma heating during magnetic reconnection, including effective heating (Drake et al., 2009; Drake and Swisdak, 2014; Usami et al., 2017; Usami et al., 2019a; Usami et al., 2019b). Non-Maxwellian velocity distributions themselves are the smoking gun demonstrating effective heating based on kinetic effects. In 2009, Drake et al. showed that only heavy ions as minor ion components behave nonadiabatically and are effectively heated in magnetic reconnection, presuming that the proton is the main ion component (Drake et al., 2009; Drake and Swisdak, 2014). In 2017, we have demonstrated that a large part of protons as the main ion component behave nonadiabatically and have discovered ring-shaped velocity distributions of protons in particle simulations (Usami et al., 2017; Usami et al., 2019a; Usami et al., 2019b). Although Drake et al. called the above process "the pickup," it is different from the classic pickup, which was directly discovered by Möbius et al. (Möbius et al., 1985). In the classical pickup, newly ionized particles create a ring velocity distribution, while in the "novel" pickup of Drake et al., heavy ions (not newly ionized) are nonadiabatic upon crossing the separatrix and they are equivalent to the freshly ionized particles in the aspect of behaviors. In this paper, let us call our process "the pickup-like process." The relationship among the classical pickup, the novel pickup, and the pickup-like process is so complicated that more details have been summarized in Ref. (Usami et al., 2019b).

On the other hand, from a different perspective, ring-shaped velocity distributions have been investigated by theories and numerical analysis, since a ring-shaped velocity distribution is unstable and generates various waves. Wu and Davidson derived the dispersion relation and the growth rate of an excited wave in the presence of a ring velocity distribution, assuming a negligible spread in velocities (Wu and Davidson, 1972). This case corresponds to a ring-shaped distribution with no width. As a general case of rings, many researchers, for instance, Ashour-Abdalla et al., Thorne et al., and Wu et al., addressed a ring-shaped distribution with a finite width (Ashour-Abdalla and Kennel, 1978; Thorne and Summers, 1989; Wu et al., 1989). After that, Mithaiwala et al. discussed a ring velocity distribution in a multi-ion component plasma (Mithaiwala et al., 2010), and Winske et al. explored a ring distribution not only from theories but also by using simulations (Winske and Daughton, 2012). Because they focused on the nature of instabilities generated from ring distributions, they assumed specific shapes of a ring with a width and invented model functions to fit the assumed shape; the formation mechanism of the model functions was not up for discussion. As model functions of a ring with a width, Ashour-Abdalla et al. chose "the subtracted Maxwellian" $\exp(-v_\perp^2/a_\perp^2) - \exp(-v_\perp^2/(\beta a_\perp)^2)$ (Ashour-Abdalla and Kennel, 1978), Thorne et al. adopted a function of $(v_\perp/a_\perp)^{2l}\exp(-v_\perp^2/a_\perp^2)$ (Thorne and Summers, 1989), and Wu et al. employed a function of $\exp(-(v_\perp - v_0)^2/a_\perp^2)$ (Wu et al., 1989). These model functions would be sufficiently accurate, under the condition that the ring's radius is much larger than the width.

In contrast, in this work we theoretically derive a function which exactly expresses ring-shaped velocity distributions with a finite width created through the pickup-like process, assuming a steady feeding of Maxwellian populations and a mixing of gyration phases. Moreover, the most remarkable conclusion to emerge from this work is that when the width of a ring, which is defined as the standard deviation of the fed Maxwellian populations, is larger than a criterion, the distribution shape changes from a ring into a mountain. We name such a mountain-shaped distribution "a pseudo-Maxwellian velocity distribution," because the mountain shape is so similar to the shape of a Maxwellian distribution that the two shapes are almost indistinguishable from each other.

The organization of this paper is as follows. In **Section 2**, we analytically obtain a function which exactly expresses a ring-shaped velocity distribution with a finite width. It is shown that under a certain condition, the local minimum of a ring's center is changed to be the maximum, that is, the peak of a mountain-like structure. Consequently a pseudo-Maxwellian velocity distribution is formed. In **Section 3**, we introduce our particle simulation model in an open system for magnetic reconnection in the presence of a guide magnetic field. In **Section 4**, as results of the particle simulation, we show ion velocity distributions and the dependence of the distribution shape on the guide magnetic field. Furthermore, we discuss physics contributing to the formation of a ring's width. In **Section 5**, we carry out test particle simulations, in which the motions of ions are calculated in an electromagnetic field given by a particle simulation run. It is confirmed in **Section 4.2** and in **Section 5** that the ion velocity distributions found in

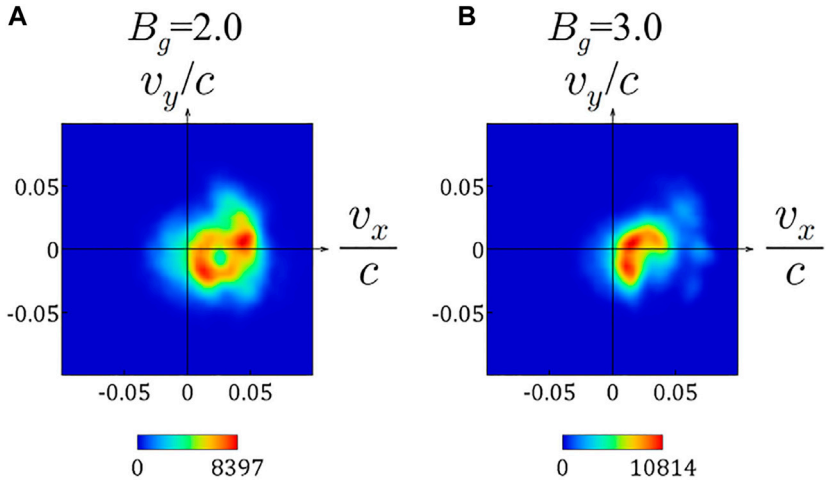


FIGURE 1 | Ion velocity distributions obtained by particle simulations in previous works **(A)**: a circle -shaped structure is formed in a $B_g = 2.0$ case **(B)**: a circular-arc-shaped structure is formed in a $B_g = 3.0$ case.

the above particle simulation are surely pseudo-Maxwellian distributions. As discussion and suggestion, in **Section 6**, we explain an unsolved issue in the formation of pseudo-Maxwellian distributions. In addition, we suggest that our findings have a potential to affect existing knowledge based on simulation or observation data and to be applicable to other phenomena. **Section 7** provides a summary of this work.

2 THEORY

Before describing this work, we review the formation theory of circle-shaped and circular-arc-shaped velocity distributions in magnetic reconnection, which is the foundation for the theory of pseudo-Maxwellian velocity distributions. Recently, by particle simulation we have discovered a circle-shaped velocity distribution of ions as shown in **Figure 1A** for $B_g = 2.0$ and an arc-shaped distribution as shown in **Figure 1B** for $B_g = 3.0$ (Usami et al., 2017; Usami et al., 2019b), where B_g is the ratio of the guide magnetic field to the antiparallel magnetic field in the far upstream. We have found a basic understanding of the formation process of such velocity distributions. A large part of ions enter the downstream from the upstream across the separatrix not passing through regions near the reconnection point. The width of the separatrix is thin for ions, and hence the ion behavior is nonadiabatic when crossing the separatrix. When the ions enter the downstream, their velocities are much less than the reconnection outflow speed $u_{\rm out}$ (in the x-direction), because the ions, whose velocities are quite small in the upstream, are not sufficiently accelerated in the separatrix. Thus we regard the entry velocity as zero in an ideal case. For simplification, we assume that in the downstream, the guide magnetic field in the z direction B_z and the convective electric field in the y direction E_y are uniform, and we ignore the other components of the electromagnetic field. Under this situation, $u_{\rm out}$ is expressed as $u_{\rm out} = cE_y/B_z$, where c is the speed of light. Considering an initial state that ions with the zero velocity are located in the above simplified downstream, we can easily grasp the motion of the ions. The ions move in the x direction owing to the $E_y \times B_z$ drift while in gyromotion around the guide magnetic field in the downstream. The drift speed is equal to $u_{\rm out}$, and the gyration speed is also equal to $u_{\rm out}$. The above explanation is based on the Lagrangian point of view. From the Eulerian point of view, there exist particles having various gyration phases in the downstream at some instant. Hence as a velocity distribution inside a small area, we can observe a circle (It is noted that the general shape is a circular-arc as shown in **Figure 1B** (Usami et al., 2019b)).

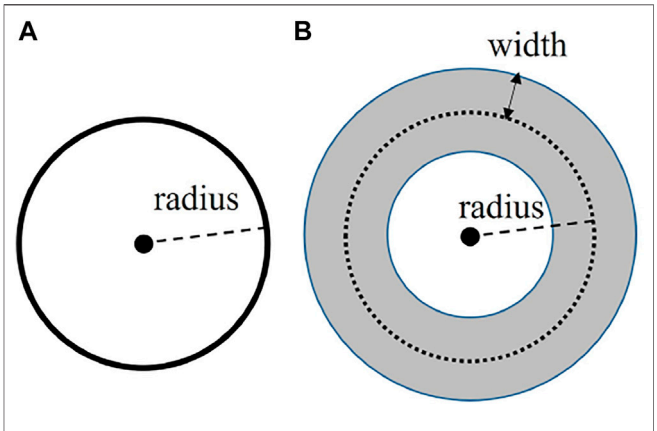


FIGURE 2 | Schematic diagrams of **(A)**: a circle, i.e., a ring with no width and **(B)**: an annulus, i.e., a ring with a finite width. Here, the radius of the dotted circle is conventionally regarded as the radius of the annulus.

Here in short we compare our previous works and this work, and clearly state the difference. In the previous works (Usami et al., 2017; Usami et al., 2019a; Usami et al., 2019b), we have ignored a ring's width as drawn in **Figure 2A**. In this work, we consider a ring-shaped velocity distribution with a finite width, as illustrated in **Figure 2B**.

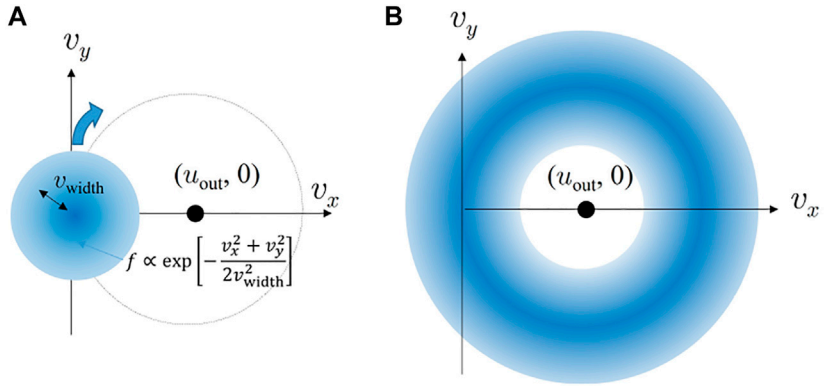


FIGURE 3 | Schematic diagrams showing that **(A)**: an initial Maxwellian distribution begins to rotate around the center (u_{out}, 0) and that **(B)**: a ring-shaped distribution with a width is newly created as a result of the rotation of the initial Maxwellian distribution.

For the purpose of use in the following theory and simulation, we extend the concept of thermal velocity and temperature to be applicable to non-Maxwellian distributions as effective thermal velocity and effective temperature. We define the effective thermal velocity of j-component $v_{\mathrm{Teff},j}$ as the standard deviation of particle velocities,

$$v_{\mathrm{Teff},j}^2 = \frac{\int \left(v_j - \langle v_j \rangle\right)^2 f d^3v}{\int f d^3v}, \tag{1}$$

where f is a velocity distribution function, v_j represents the j-component of a particle velocity, and $\langle v_j \rangle$ is the j-component of the averaged velocity. A ring (no matter if it has a width or not) is a two-dimensional structure. Thus, taking, for example, the x- and y-components as the two components in two dimensions, we define the effective thermal velocity of a ring velocity distribution as

$$v_{\mathrm{Teff}}^2 = \frac{1}{2}\left(v_{\mathrm{Teff},x}^2 + v_{\mathrm{Teff},y}^2\right). \tag{2}$$

Also, the effective ion temperature is defined as $T_i = m_i v_{\mathrm{Teff}}^2$, where m_i is the ion mass. In the case of a circle, i.e., a ring with no width as illustrated in **Figure 2A**, the effective temperature is $1/2 m_i u_{\mathrm{out}}^2$, where say the radius is u_{out}. In the case of an annulus, i.e., a ring with a width, as drawn in **Figure 2B**, the effective temperature is clearly larger than $1/2 m_i u_{\mathrm{out}}^2$, Here, it is noted that the width has the same length on the both sides of the dotted circle and conventionally the annulus's radius u_{out} is defined to be the averaged value of the outer circle's and the inner circle's radii.

The width of a ring is caused predominantly by velocity variations of ions entering the downstream, which will be discussed in **Section 4.3**. In the theories of the previous works, Refs. (Usami et al., 2017), (Usami et al., 2019a), and (Usami et al., 2019b), we have ignored the velocity variations and have supposed that all the ions have the same entry velocity (0, 0). In this work in contrast, we incorporate velocity variations of the entry velocity around (0, 0) into the theory. Here, let us point out an important key point in treatment of the width of a circle. Assuming again the uniform B_z and E_y, the orbits of the ions are circles whose center is (u_{out}, 0) in the velocity space ($u_{\mathrm{out}} = cE_y/B_z$). The key point is that the ions have the same gyroperiod, not depending on each ion velocity, while the circle size in the velocity space depends on each ion velocity. It is obvious that as an ion has higher speed perpendicular to the magnetic field, the circumference along which the ion traces is larger. This means that the density in the velocity space is inverse-proportional to the distance from (u_{out}, 0), if the same number of ions are assigned on each circumference of various concentric circles. We need always to take into account the so-called inverse-proportional effect.

Now we consider a specific case of a ring's width, in which ions satisfying a Maxwellian velocity distribution $\exp[-(v_x^2 + v_y^2)/(2v_{\mathrm{width}}^2)]$ continuously enter the downstream and rotate around the center (u_{out}, 0) as illustrated in **Figure 3A**. The velocity distribution newly created in the downstream is a ring with a width, as shown in **Figure 3B**. The effective thermal speed v_{Teff} in this case is analytically derived as

$$v_{\mathrm{Teff}}^2 = \frac{1}{2}u_{\mathrm{out}}^2 + v_{\mathrm{width}}^2. \tag{3}$$

(In Appendix of Ref. (Usami et al., 2019b), we have analyzed a case of a one-dimensional Maxwellian distribution $\exp[-v_x^2/(2v_{\mathrm{width}}^2)]$, where $v_{\mathrm{Teff}}^2 = 1/2u_{\mathrm{out}}^2 + 1/2v_{\mathrm{width}}^2$ has been derived).

Next, we calculate the new velocity distribution G (v_x, v_y) created as a result of the process that particles satisfying a Maxwellian distribution $\exp[-(v_x^2 + v_y^2)/(2v_{\mathrm{width}}^2)]$ are continuously supplied and the particles are rotated once around the point (u_{out}, 0). The function G (v_x, v_y) is obtained by integrating $\exp[-(v_x^2 + v_y^2)/(2v_{\mathrm{width}}^2)]$ on each circumference whose radius is $V = \sqrt{(v_x - u_{\mathrm{out}})^2 + v_y^2}$ and dividing the value by each circumferential length, because we can interpret the above situation to be equivalent to the following one. Initially a part of the ions were located non-uniformly on a circumference, whose radius is taken to be V. Let these ions be the Group V. If we distribute the ions of the Group V uniformly on the circumference whose radius is V for each value of V ($0 < V <$

∞), we obtain a new function depending only on V. The new function is $G(v_x, v_y)$ to be derived. Hence, the following equation holds:

$$G(v_x, v_y) = \frac{1}{2\pi V}\int_0^{2\pi}\frac{1}{2\pi v_{\mathrm{width}}^2}\exp\left[-\frac{v_x^2+v_y^2}{2v_{\mathrm{width}}^2}\right]V d\theta. \quad (4)$$

By using the polar representation with the center $(u_{\mathrm{out}}, 0)$, $v_x = u_{\mathrm{out}} + V\cos\theta$ and $v_y = V\sin\theta$,

$$G(v_x, v_y) = \frac{1}{(2\pi v_{\mathrm{width}})^2}\exp\left[-\frac{V^2+u_{\mathrm{out}}^2}{2v_{\mathrm{width}}^2}\right]\int_0^{2\pi}\exp\left[-\frac{u_{\mathrm{out}}V}{v_{\mathrm{width}}^2}\cos\theta\right]d\theta, \quad (5)$$

$$= \frac{1}{2\pi v_{\mathrm{width}}^2}\exp\left[-\frac{V^2+u_{\mathrm{out}}^2}{2v_{\mathrm{width}}^2}\right]I_0\left(\frac{u_{\mathrm{out}}V}{v_{\mathrm{width}}^2}\right), \quad (6)$$

is derived, where I_n is the modified Bessel function of the first kind. It is noted that $G(v_x, v_y)$ is dependent only on V, but $G(v_x, v_y)$ is a probability density function of the velocity vector (v_x, v_y), i.e., $G(v_x, v_y)$ is a distribution function on two-dimensional space (v_x, v_y). On the other hand, by virtue of the axisymmetric structure of $G(v_x, v_y)$, the cross-sections of $G(v_x, v_y)$ have the same profile for any line crossing the center $(u_{\mathrm{out}}, 0)$. In the following discussion, thus, we use the cross-section function of the newly formed distribution

$$F(v) = \frac{1}{2\pi v_{\mathrm{width}}^2}\exp\left[-\frac{v^2+u_{\mathrm{out}}^2}{2v_{\mathrm{width}}^2}\right]I_0\left(\frac{u_{\mathrm{out}}v}{v_{\mathrm{width}}^2}\right), \quad (7)$$

where $-\infty < v < \infty$.

By analyzing **Eq. 7**, we show that the shape of the newly formed velocity distribution significantly changes depending on u_{out} and v_{width} and derive necessary conditions for the distribution to be a pseudo-Maxwellian distribution. For this purpose, we investigate whether the profile has a dip[1], in other words, a local minimum in the center. It can be said that if $F(v)$ has a dip in the center, it is not a pseudo-Maxwellian distribution, while if $F(v)$ does not have a dip, it is a pseudo-Maxwellian one. We treat $F(v)$ only for $v > 0$, because $F(v)$ is an even function. We can find that $F \to 0$ for $v \to \infty$ and F monotonically decreases in the regime of $v \gg v_{\mathrm{width}}$. Hence, whether F has a dip or not depends on the sign of dF/dv in the vicinity of $v = 0$. If dF/dv is positive at $v \simeq 0$, F has a dip. Differentiating F with respect to v, we have

$$\frac{dF}{dv} = \exp\left[-\frac{v^2+u_{\mathrm{out}}^2}{2v_{\mathrm{width}}^2}\right]\left[-\frac{v}{v_{\mathrm{width}}^2}I_0\left(\frac{u_{\mathrm{out}}v}{v_{\mathrm{width}}^2}\right)+\frac{dI_0}{dv}\left(\frac{u_{\mathrm{out}}v}{v_{\mathrm{width}}^2}\right)\right]. \quad (8)$$

By using formulas of the modified Bessel function of the first kind, $dI_0(x)/dx = I_1(x)$, and the following approximation by Taylor expansion in the vicinity of $x = 0$, $I_0(x) = 1 + (dI_0/dx)(0)x + \cdots \simeq 1$ and $I_1(x) = 0 + (dI_1/dx)(0)x + \cdots \simeq 1/2x$, we obtain

[1]If $v_{\mathrm{width}} = 0$, $F = 0$ at $v = 0$, and the ring center is "a hole." In genera cases of $v_{\mathrm{width}} \neq 0$, $F > 0$ at $v = 0$, and thus we call the ring center "a dip."

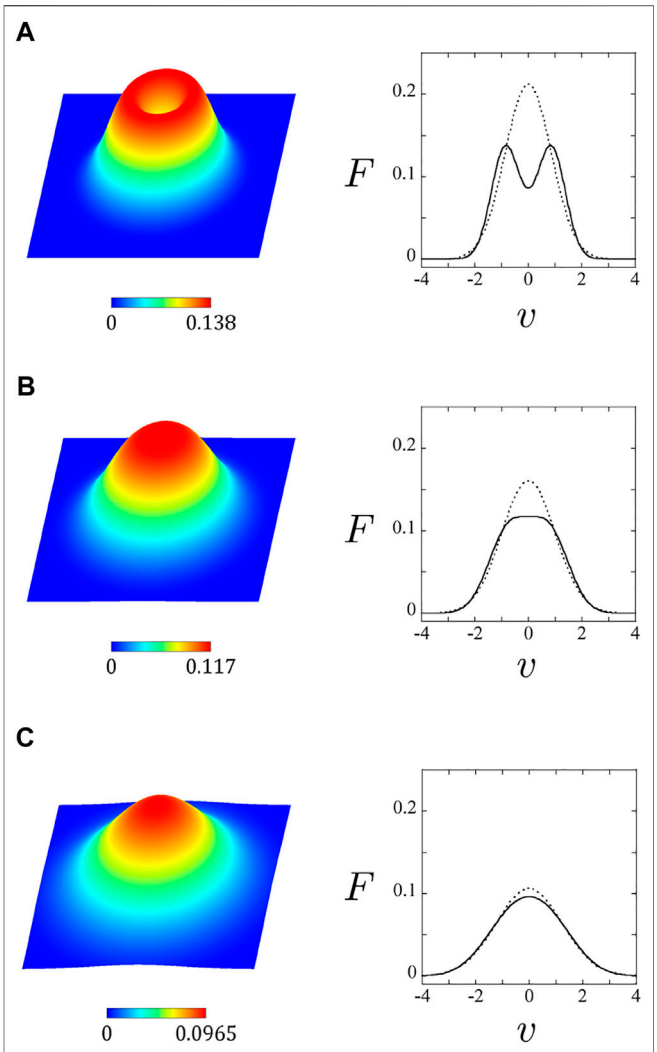


FIGURE 4 | The left panels depict a bird's eye view of the function $G(v_x, v_y)$ and the right panels plot graphs of the function $F(v)$ expressing the cross-section of $G(v_x, v_y)$ **(A)**: $v_{\mathrm{width}} = 0.5$ **(B)**: $v_{\mathrm{width}} = 0.7$, and **(C)**: $v_{\mathrm{width}} = 1.0$ are assigned, while keeping $u_{\mathrm{out}} = 1.0$.

$$\frac{dF}{dv} \simeq -\exp\left[-\frac{v^2+u_{\mathrm{out}}^2}{2v_{\mathrm{width}}^2}\right]\left(\frac{v}{v_{\mathrm{width}}^4}\right)\left(v_{\mathrm{width}}^2-\frac{1}{2}u_{\mathrm{out}}^2\right). \quad (9)$$

This equation clearly indicates that if the condition

$$v_{\mathrm{width}} > \frac{u_{\mathrm{out}}}{\sqrt{2}}, \quad (10)$$

is satisfied, dF/dv is negative in the vicinity of $v = 0$, that is, F does not have a dip in the center. Accordingly, we can expect that the newly created distribution is a pseudo-Maxwellian distribution. In contrast, when $v_{\mathrm{width}} < u_{\mathrm{out}}/\sqrt{2}$, dF/dv is positive in the vicinity of $v = 0$. The velocity distribution has a dip, and hence a pseudo-Maxwellian distribution is not formed.

In **Figure 4**, we depict a bird's eye view of the distribution function $G(v_x, v_y)$ in the left panels and the cross-section function $F(v)$ in the right panels. We set $v_{\mathrm{width}} = 0.5$, 0.7, and 1.0, for cases

of **Figures 4A–C**, respectively, while we assign $u_{out} = 1.0$ for all the cases. In each right panel, the solid line represents $F(v)$, and the dotted line indicates a Maxwellian distribution function which has the standard deviation equal to the one of $F(v)$. In **Figure 4A**, we can find that the profile has a dip, and thus a ring-shaped distribution holds. In **Figure 4B**, there is not a dip, but there is a plateau in the center of the profile. This is because v_{width} is nearly equal to $u_{out}/\sqrt{2}$ and hence the gradient in the vicinity of the center is nearly equal to zero, as predicted by **Eq. 9**. In the case of **Figure 4C**, we can see that the shape becomes a mountain-like structure, which almost fits with a Maxwellian distribution. In what follows, we call such distributions with no dip for $v_{width} > u_{out}/\sqrt{2}$ pseudo-Maxwellian velocity distributions. One likely can not distinguish a pseudo-Maxwellian distribution and a genuine-Maxwellian distribution, alone by observing the shapes.

Lastly in this section, we excuse a slight lack of precision in the discussion of the newly created velocity distribution. This is responsible for complexity in explaining the bridge of the Lagrangian point of view (the individual particle motion) and the Eulerian point of view (the velocity distribution). From the Lagrangian viewpoint, the particle motion is $E \times B$ drift while in gyromotion, and the orbits in the velocity space (v_x, v_y) are circles. From the Eulerian viewpoint, we focus on a small local area whose size is much smaller than the Larmor radius of particles whose gyration speed is u_{out}. Thus, not the entire trajectory of a certain particle is contained inside the small area. We have stated as if the newly formed distribution is composed of the entire orbits of particles, but this physical picture is not correct in a precise sense. The exact physical picture is that the velocity distribution is composed of particles inside a local area at a certain moment, which particles have various gyration phases, because of a mixing of gyration phases. For the sake of convenience, we have described the formation process of a velocity distribution from the Lagrangian point of view, but the essential part of the theory has been maintained.

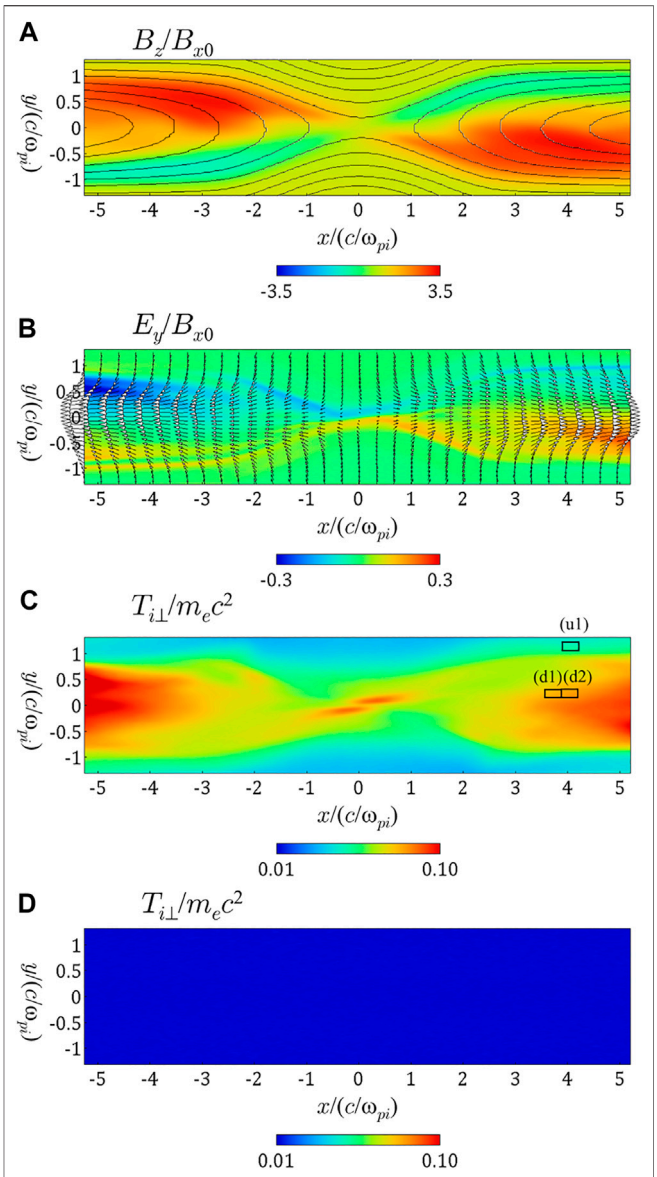


FIGURE 5 | Spatial profiles of **(A)**: B_z and the magnetic field lines **(B)**: the ion bulk velocity vectors and E_y **(C)** and **(D)**: the ion temperature perpendicular to the magnetic field. The panels **(A)**–**(C)** display results at $\omega_{pi}t = 775$, and the panel **(D)** shows a result at the initial time.

3 PARTICLE SIMULATION METHOD

We search for pseudo-Maxwellian velocity distributions in collisionless driven magnetic reconnection in the presence of a guide magnetic field by means of two-dimensional electromagnetic particle-in-cell (PIC) simulations, using "PASMO" (Horiuchi and Sato, 1997; Pei et al., 2001a; Pei et al., 2001b; Ohtani and Horiuchi, 2009).

In PASMO, an open boundary condition is employed. At the upstream boundary ($y = \pm y_b$), in order to generate plasma inflows and magnetic fluxes, an external driving electric field E_d is imposed in the direction perpendicular to the magnetic field (The terms of "perpendicular" and "parallel" indicate perpendicular and parallel to the magnetic field at each position, not to the averaged or initial magnetic field.) The driving electric field E_d is set to zero at the initial time and begins to grow first near the center of the upstream boundary ($x = 0$, $y = \pm y_b$). The inflow region where E_d is imposed expands in the $\pm x$ directions with a speed of $1.2v_{A,up}$, where $v_{A,up}$ is the Alfvén speed for the antiparallel magnetic field at the upstream boundary. Eventually E_d develops to reach $E_{dz} = -0.04B_{x0}$ in the entire upstream boundary, where E_{dz} is the z-component of E_d. As E_d grows, the magnetic field at the upstream boundary rises according to Faraday's law. In addition, $E_x = 0$ and $\partial E_y/\partial y = 0$ are applied at the upstream boundary. At the upstream boundary, every time step, all the particles are removed and particles are freshly set which satisfy a shifted Maxwellian velocity distribution, whose averaged velocity is equal to the $E \times B$ drift velocity. The plasma density at the upstream boundary is adjusted to be proportional to the magnetic field strength so that the frozen-in constraint holds at the upstream boundary. By this procedure, particles are continuously supplied from the upstream

boundary into the simulation domain. In contrast, the downstream boundary ($x = \pm x_b$) is taken to be free, across which particles can freely go in and out. Some technical methods are implemented into PASMO in order for particles with a distribution to continuously and smoothly cross the downstream [for detail, see (Ohtani and Horiuchi, 2009)]. On the following components of the electromagnetic field, the conditions $\partial E_x/\partial x = \partial B_y/\partial x = \partial B_z/\partial x = 0$ are imposed. The other components of the electromagnetic field are derived by solving Maxwell's equations at the downstream boundary.

As the initial condition, we take a one-dimensional Harris-type equilibrium with an antiparallel magnetic field in the x direction B_x and a uniform guide magnetic field in the z direction B_z. Thus, the initial state is expressed as

$$B_x(y) = B_{x0}\tanh(y/L), \tag{11}$$

$$B_z(y) = B_{z0}, \tag{12}$$

$$P(y) = P_0 + B_{x0}^2/(8\pi)\mathrm{sech}^2(y/L), \tag{13}$$

where P represents the plasma pressure. The quantities B_{x0}, B_{z0}, and P_0 are constants, and L is a spatial scale in the y-axis. The initial particle velocity distribution is a shifted Maxwellian distribution with spatially uniform temperature. The initial ion temperature is taken to be equal to the initial electron temperature.

The simulation parameters are as follows. The simulation domain size is $2x_b \times 2y_b = (15.81 \times 2.63)c/\omega_{pi}$, where ω_{pi} is the ion plasma frequency. The plasma frequency is defined by the use of the initial number density at the neutral line $y = 0$, n_0. The initial number of electrons and the initial number of ions are 28 182 528, respectively. The ion-to-electron mass ratio is taken to be $m_i/m_e = 100$, i.e., a reduced mass ratio is used (The influence of the mass ratio on the pickup-like process has been discussed in Ref. (Usami et al., 2019b). In a short conclusion, it is theoretically predicted that the pickup-like process works better under the real mass ratio.) The ratio of the electron plasma frequency to the electron gyrofrequency is $\omega_{pe}/\omega_{ce} = 6.0$, where we define $\omega_{ce} = eB_{x0}/(m_e c)$. The Alfvén speed for B_{x0} and n_0 is $v_{A0}/c = 0.017$. The time step is $\omega_{pi}\Delta t = 0.0052$, and the grid spacing is $\Delta_g/(c/\omega_{pi}) = 0.010$.

4 PARTICLE SIMULATION RESULT

4.1 Pseudo-Maxwellian Velocity Distribution

We perform a particle simulation run under the conditions of $B_g = B_{z0}/B_{x0} = 1.0$, $L/(c/\omega_{pi}) = 0.66$, and $P_0/(B_{x0}^2/8\pi) = 0.35$. In **Figures 5A–C**, we display simulation results in the region of $-5.27 < x/(c/\omega_{pi}) < 5.27$ at $\omega_{pi}t = 775$ and in **Figure 5D** we show a simulation result at the initial time, where the electromagnetic field, the velocity, and the temperature are normalized to B_{x0}, c, and $m_e c^2$, respectively. By $\omega_{pi}t = 775$ the reconnection electric field is balanced with the driving electric field E_{dz} imposed at the upstream boundary, and the reconnection system is in a quasi-steady state. **Figure 5A** shows the spatial profile of the out-of-plane component of the magnetic field B_z as color contours and magnetic field lines. Magnetic reconnection is driven by plasma inflows and magnetic fluxes supplied from the upstream boundary, and the reconnection point, the X-point, is located at the center of the simulation domain (0, 0). The out-of-plane component of the magnetic field consists of the initial guide field B_{z0} and the quadrupole magnetic field generated by the Hall current. As a result, B_z is positive in the main part of the downstream, although B_z is negative in small parts. **Figure 5B** shows the ion bulk velocity vectors as arrows and the y-component of the electric field E_y as color contours. From the velocity vectors, we can see that bipolar reconnection outflows emanate from the X-point, and from the E_y profile, we can find that E_y is produced in the entire downstream as the dominant component of the convective electric field. **Figures 5C,D** depict the spatial profiles of the ion temperature perpendicular to the magnetic field $T_{i\perp}$ at $\omega_{pi}t = 775$ and at $\omega_{pi}t = 0$, respectively. It is clearly seen that the ion temperature rises mainly in the downstream at $\omega_{pi}t = 775$, comparing **Figure 5C** with **Figure 5D**.

In **Figures 6A,B**, we show ion velocity distributions taken at the boxed areas (d1) and (d2) designated in **Figure 5C**, respectively. Unlike the cases of $B_g = 2.0$ and 3.0 introduced in **Figure 1**, we can see that instead of a circle-shaped or an arc-shaped structure, mountain-shaped velocity distributions, which are the central part near $(v_x, v_y) = (0, 0)$, are formed. These velocity distributions are too similar to a Maxwellian distribution to be distinguishable in shape, and thus we interpret them to be pseudo-Maxwellian distributions as described in **Section 2**. Here, **Figure 6** indicates that an additional structure is attached to the right part of each pseudo-Maxwellian distribution. It is a horn-shaped distribution discussed in Ref. (Usami et al., 2019a), which is a kind of circular-arc-shaped velocity distribution. The formation process of horn-shaped velocity distributions is explained by an extended theory of the pickup-like process. For details, refer to Ref. (Usami et al., 2019a).

We almost conclude that the mountain-like distributions shown in **Figure 6** are pseudo-Maxwellian distributions, i,e., ring-shaped distributions with an extremely large width, based on the existing of an additional horn-shaped structure, which also is created by the pickup-like process. However, an intriguing property of the pseudo-Maxwellian distributions, that the shape is quite similar to the genuine-Maxwellian shape, acts as a negative aspect, when rigorously determining whether a mountain-like distribution is a pseudo-Maxwellian or a genuine-Maxwellian distribution in particle simulations. Although pseudo-Maxwellian and genuine-Maxwellian distributions are theoretically expressed by obviously different functions, it is practically impossible for particle simulations to directly detect the deference so as to distinguish the two. In particle (particle-in-cell) simulations, including PASMO, employing the super-particle method (Birdsall and Langdon, 1991), the number of particles are much less than that in actual plasmas. Thus, statistical fluctuations are inevitably contained in velocity distributions. In addition, other physical effects could affect the shape of velocity distributions for this case, which will be shortly described in **Section 6**. Accordingly, alone by using the simulation results shown in **Section 4.1**, we can not completely

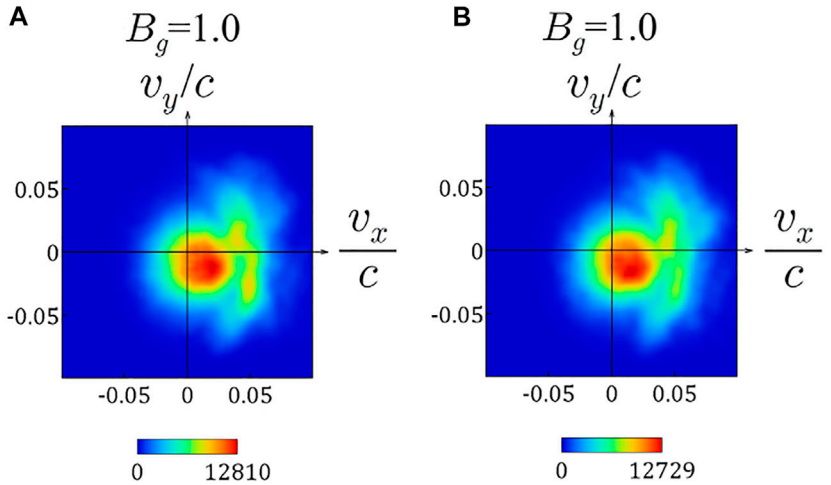


FIGURE 6 | Ion velocity distributions **(A)**: in the boxed area (d1) and **(B)**: in the boxed area (d2) indicated in **Figure 5C**. In both panels, pseudo-Maxwellian distributions are seen at the central part near (v_x, v_y) = (0, 0).

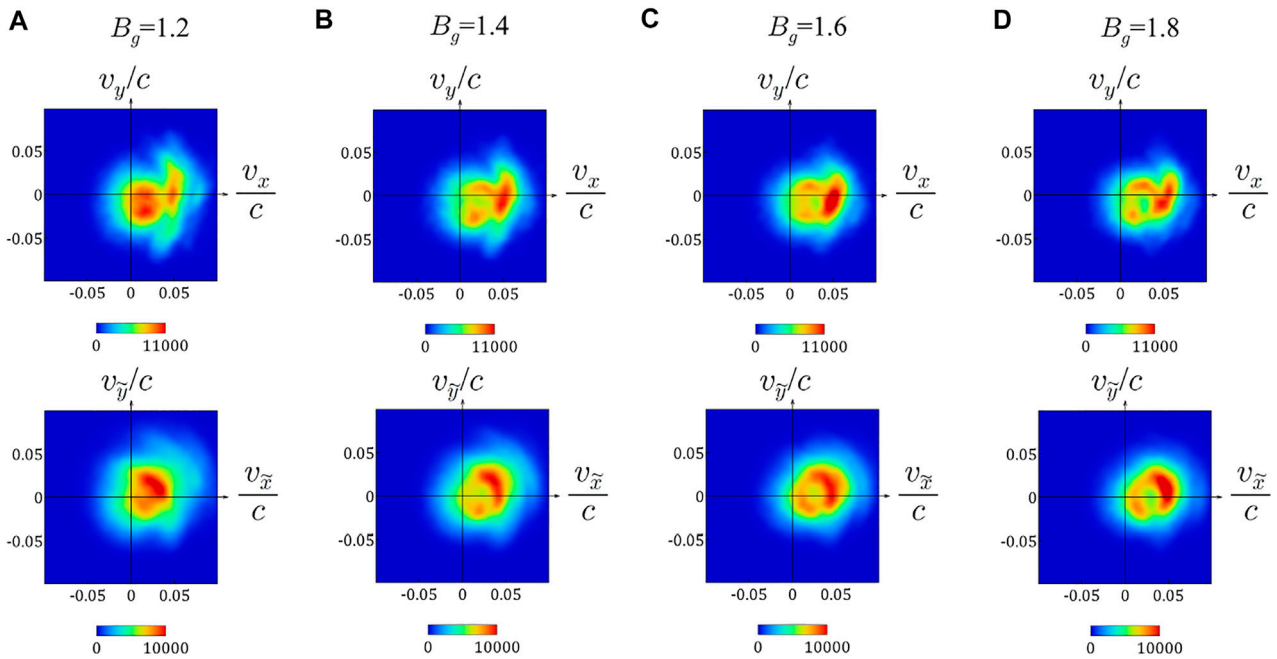


FIGURE 7 | Ion velocity distributions for various values of the guide field ratio B_g **(A)**: B_g = 1.2 **(B)**: B_g = 1.4 **(C)**: B_g = 1.6, and **(D)**: B_g = 1.8. The upper panels are taken in the (v_x, v_y) plane, and the lower panels are taken in the ($v_{\tilde{x}}$,$v_{\tilde{y}}$) plane.

deny that the distributions shown in **Figure 6** might be genuine-Maxwellian distributions. In **Section 4.2** and in **Section 5**, we demonstrate two kinds of evidence to conclude that the distributions in **Figure 6** are pseudo-Maxwellian distributions, and furthermore to lead to implication that pseudo-Maxwellian distributions would be frequently formed in some cases of magnetic reconnection with a guide field.

4.2 Guide Field Dependence (Evidence 1)

In order to more definitely demonstrate that the distributions found in **Figure 6** are pseudo-Maxwellian distributions, we carry out a series of particle simulations and investigate the dependence of the shape of ion velocity distributions on the guide magnetic field. We show velocity distributions in the (v_x, v_y) plane and in the ($v_{\tilde{x}}$,$v_{\tilde{y}}$) plane, where $\tilde{x}$ and $\tilde{y}$ are two directions which are mutually perpendicular and are perpendicular to the magnetic

field. The reason is as follows. If a ring-shaped velocity distribution is formed, it is clearly observed in the $(v_{\tilde{x}}, v_{\tilde{y}})$ plane, because a ring is created as a result of the gyration. If the out-of-plane component of the magnetic field is dominant, the (x, y) plane is nearly perpendicular to the magnetic field so that the (v_x, v_y) plane is almost equal to the $(v_{\tilde{x}}, v_{\tilde{y}})$ plane. In Refs. (Usami et al., 2017) and (Usami et al., 2019b), we have displayed velocity distributions in the (v_x, v_y) plane for cases of high guide-field such as B_g = 2–4. In this work, however, we show results mainly for B_g = 1–2, and thus add velocity distributions in the $(v_{\tilde{x}}, v_{\tilde{y}})$ plane. Let us define $v_{\tilde{x}} = \boldsymbol{v} \cdot (\boldsymbol{E}_\perp \times \boldsymbol{B})/(E_\perp B)$, $v_{\tilde{y}} = \boldsymbol{v} \cdot \boldsymbol{E}_\perp / E_\perp$, and $v_{\tilde{z}} = \boldsymbol{v} \cdot \boldsymbol{B}/B$, where $\boldsymbol{E}_\perp$ is the perpendicular component of $\boldsymbol{E}$ to $\boldsymbol{B}$, i.e., $\boldsymbol{E}_\perp = \boldsymbol{E} - [\boldsymbol{E}\cdot\boldsymbol{B}/B]\boldsymbol{B}/B$.

Figures 7A–D show ion velocity distributions for cases of B_g = 1.2, 1.4, 1.6, and 1.8, respectively. The upper and lower panels represent velocity distributions in the (v_x, v_y) plane and in the $(v_{\tilde{x}}, v_{\tilde{y}})$ plane, respectively. The locations of the area for the panels (A)-(D) are the same as the one for **Figure 6B**. It is found from the panel (A) that a ring-shaped structure is not seen, but a mountain-like structure is seen in the case of B_g = 1.2. In contrast, according to the panels (B)-(D), as B_g is larger, we can observe a clearer ring. To quantify the clearness of rings, we extract each one-dimensional profile along the v_y-axis crossing the center of a mountain or a ring from the panels (A)-(D) and obtain each best-fit Gaussian (Maxwellian distribution) curve based on regression analysis. The values of the coefficient of determination R^2 for the panels (A)-(D) are 0.987, 0.952, 0.945, and 0.889, respectively, which indicates that the shape is close to the Maxwellian function in the order of (A) (B) (C), and (D). It can be said that the clearness of rings is in the order of (D) (C) (B), and (A). Next, we can find that the rings are clear in the $(v_{\tilde{x}}, v_{\tilde{y}})$ plane, compared with in the (v_x, v_y) plane, as we predict. From the velocity distributions seen in the $(v_{\tilde{x}}, v_{\tilde{y}})$ plane, we can surely grasp that ring-shaped structures are formed only for B_g = 1.4, 1.6, and 1.8. (Note that horn-shaped distributions overlap ring-shaped or pseudo-Maxwellian structures. As a consequence, the density is extensively increased only in the overlapping part. If the upper limit of the color contours is taken to be the maximum value for each panel as displayed in **Figure 7**, the ring sharpness is no longer in the order of the panel (D) (C) and (B), which leads to misunderstanding. We, therefore, use a common upper limit among the upper panels and a common upper limit among the lower panels, respectively.)

Described from the opposite viewpoint, as B_g is decreased, the ring-shaped structure gradually becomes ambiguous. In other words, it is not sudden that the ring disappears when B_g = 1.0. Hence, the following interpretation is plausible. The pickup-like ion motion, which forms a ring-shaped velocity distribution, does work for B_g = 1.0. In **Figure 6**, rings exist, but the width is so large that the dip of the ring's center is plugged and the peak of a mountain is formed in the center. Therefore in conclusion, the velocity distributions in **Figure 6** are pseudo-Maxwellian distributions.

4.3 Physics of a Ring's Width

We discuss what kind of process causes the width of ring-shaped velocity distributions. The initial thermal velocity surely plays a role, and in addition it is believed that compressional heating inside the upstream predominantly contributes to the formation of a ring's width. In what follows, we demonstrate that v_{width} corresponds to (genuine) thermal velocity in the upstream $v_{T,\mathrm{up}}$, which depends on the guide magnetic field. In the following description, we use **Eq. 10** substituting $v_{T,\mathrm{up}}$ into v_{width}.

Let us compare the spatial profiles of the ion temperature at $\omega_{pi}t$ = 775 and at the initial time in **Figures 5C,D**. We can see that at $\omega_{pi}t$ = 775, the ion temperature is increased not only in the downstream but also in the upstream, although the temperature increment in the upstream is much less than that in the downstream. **Figures 8A,B** show ion velocity distributions at $\omega_{pi}t$ = 775 and at the initial time, respectively, in the boxed area (u1), which is in the upstream. In both cases, Maxwellian distributions are satisfied, while the thermal speed is clearly larger at $\omega_{pi}t$ = 775 than that at the initial time. This indicates that in terms of fluid dynamics, compressional heating occurs in the upstream, because plasmas and magnetic fluxes are continuously injected from the upstream in our particle simulations. Furthermore, in **Figure 8C** we depict an ion velocity distribution at the same position at $\omega_{pi}t$ = 775 in a case of B_g = 2.0. Comparing **Figures 8A,C**, we can find that the ion thermal speed for B_g = 2.0 is smaller than that for B_g = 1.0. In the upstream, the ion thermal speed is $\sqrt{B_{\mathrm{up}}/B_0}$ times larger than the initial one, where B_{up} and B_0 are the magnetic field at a certain time and at the initial time, because the conservation of the magnetic moment approximately holds. Thus, we infer that as the initial magnetic field B_{z0} is larger, that is, as the guide magnetic field is larger, the compressional heating tends to be weaker.

In **Figure 9**, we plot the values of the ion thermal speed in the upstream $v_{T,\mathrm{up}}$ (the blue solid line) and the reconnection outflow speed u_{out} (the black solid line) observed in the particle simulations for various values of B_g. In order to refer to velocity distributions in the areas (d1) and (d2) of **Figure 5C**, we observe the value of u_{out} around the areas (d1) and (d2), because the outflow speed depends to some extent on the position in the downstream. Here, we regard that u_{out} is the x-component of the ion bulk velocity averaged over the region of $3.5 < x/(c/\omega_{pi}) < 5.0$ and $0.0 < y/(c/\omega_{pi}) < 0.5$ inside the downstream, and as $v_{T,\mathrm{up}}$ we use the ion thermal velocity averaged over the region of $|x/(c/\omega_{pi})| < 6.0$ and $|y/(c/\omega_{pi})| > 1.0$ inside the upstream. As B_g is larger, $v_{T,\mathrm{up}}$ becomes smaller. In contrast, as B_g is larger, u_{out} become larger, because the change in B_g affects the density and the reconnection magnetic field in the upstream. For comparison, we plot $u_{\mathrm{out}}/\sqrt{2}$ as the black dashed line. When B_g = 1.0, $v_{T,\mathrm{up}}$ is greater than $u_{\mathrm{out}}/\sqrt{2}$, and when B_g = 1.2, $v_{T,\mathrm{up}}$ is very close to $u_{\mathrm{out}}/\sqrt{2}$, although $v_{T,\mathrm{up}}$ is slightly less than $u_{\mathrm{out}}/\sqrt{2}$. Hence, as shown in **Figure 6** and **Figure 7A**, ring-shaped velocity distributions are not seen. In contrast, because $v_{T,\mathrm{up}} < u_{\mathrm{out}}/\sqrt{2}$ is sufficiently satisfied for $B_g > 1.4$, we can see ring-shaped velocity distributions, as shown in **Figures 7B–D**.

5 TEST PARTICLE SIMULATION (EVIDENCE 2)

In order to further prove that the mountain structures shown in **Figure 6** are rings with a large width, i.e., pseudo-Maxwellian

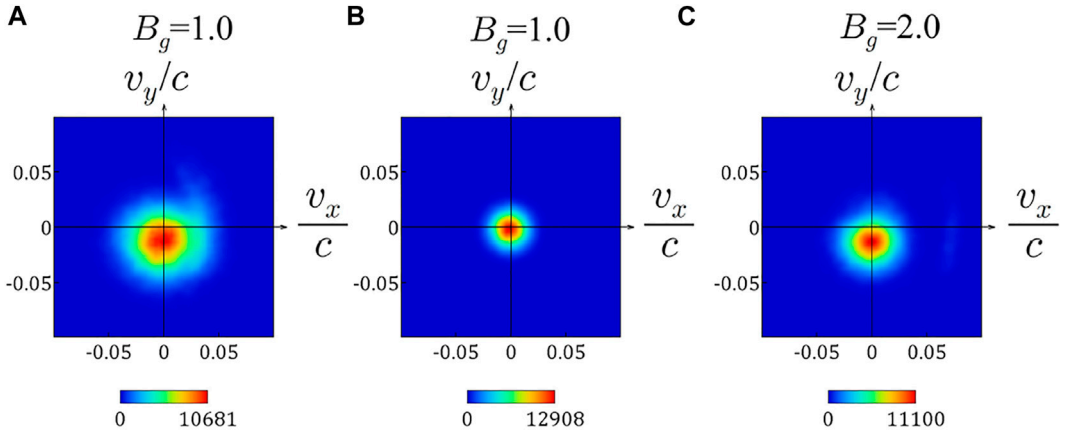


FIGURE 8 | Ion velocity distributions **(A)**: in the boxed area (u1) designated in **Figure 5C** at $\omega_{pi}t$ = 775 for B_g = 1.0 **(B)**: at the initial time, and **(C)**: in the area (u1) at $\omega_{pi}t$ = 775 for a different simulation run of B_g = 2.0.

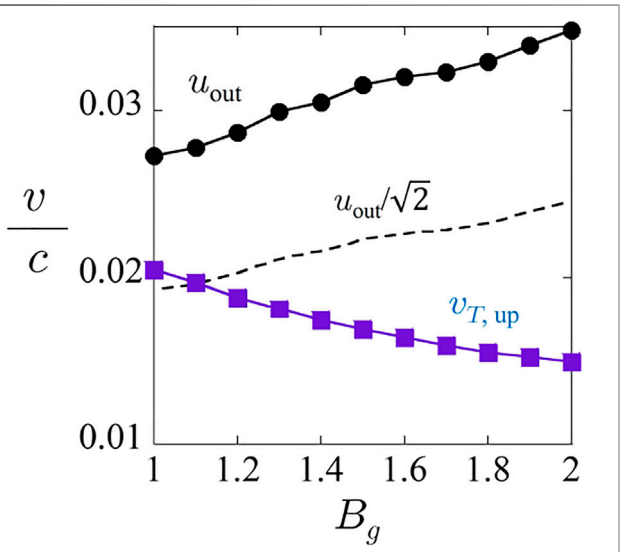


FIGURE 9 | Reconnection outflow velocity u_{out} (the black solid line) and ion thermal velocity in the upstream $v_{T,up}$ (the blue solid line) for various values of the guide field ratio B_g. For comparison, $u_{out}/\sqrt{2}$ (the black dashed line) is added.

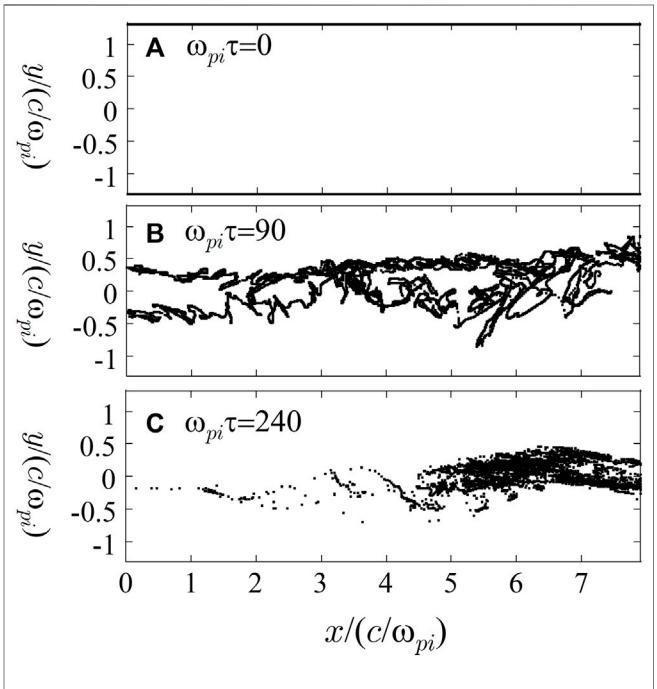


FIGURE 10 | Positions of the ions calculated by a test particle simulation **(A)**: at $\omega_{pi}\tau$ = 0 **(B)**: at $\omega_{pi}\tau$ = 90, and **(C)**: at $\omega_{pi}\tau$ = 240.

distributions, we perform a test particle simulation (Usami et al., 2019a). The method of the test particle simulation is as follows. Before the test particle simulation, we perform a particle simulation run by using the above particle simulation model, PASMO and obtain data of an electromagnetic field at some instant, which corresponds to magnetic reconnection in a quasi-steady state. In the test particle simulation, the equations of motion for test particles are solved in the electromagnetic field given by the particle simulation. In the following run of the test particle simulation, as the given field, we use the electromagnetic field at $\omega_{pi}t$ = 775 for B_g = 1.0, as displayed in **Figures 5A,B**.

We demonstrate the positions of the ion particles at various times (A) $\omega_{pi}\tau$ = 0 (B) 90, and (C) 240 in **Figure 10**. For distinguishing the time in the test particle simulation from the time in the particle simulations, we use τ as the time in the test particle simulation. The panel (A) shows that the test ions are set in the area of $0 < x/(c/\omega_{pi}) < 7.91$ on the upstream boundary $y/(c/\omega_{pi}) = \pm 1.31$. The number of test ions is 60 000, and we set 30 000 ions on the line $y/(c/\omega_{pi}) = 1.31$ and 30 000 ions on the line $y/(c/\omega_{pi}) = -1.31$. Initially, each test ion is set to have a velocity equal to the ion fluid velocity at each position. At $\omega_{pi}\tau$ = 90 (the panel (B)), the ions have entered the downstream from the upper- and lower-sides of the

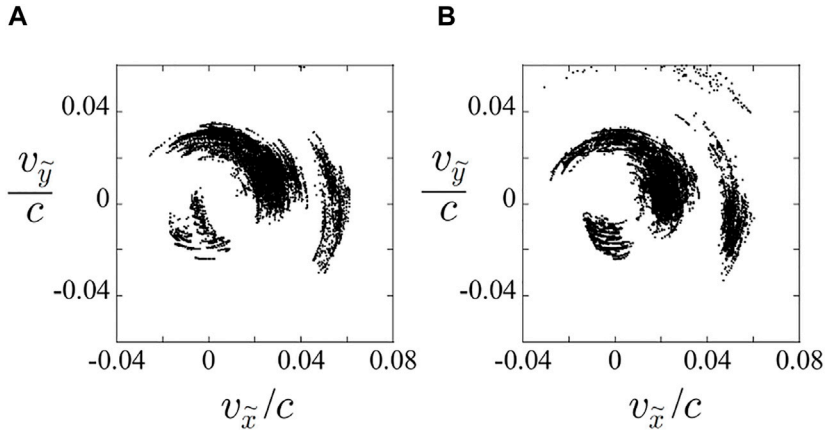


FIGURE 11 | Velocities $(v_{\tilde{x}}, v_{\tilde{y}})$ of the ions inside small areas whose locations are the same as **(A)**: the boxed area (d1) and **(B)**: the boxed area (d2) represented in **Figure 5C**, respectively.

upstream boundary. After that, the ions move in the x direction, and then at $\omega_{pi}\tau = 240$ (the panel (C)), some ions have already escaped from the simulation domain across the downstream boundary $x/(c/\omega_{pi}) = 7.91$. The test particle simulation run is terminated at $\omega_{pi}\tau = 300$.

Under a steady state of reconnection, particles continuously flow inward from the upstream with a constant flux. In the test particle simulation, however, we do not assign new particles at the upstream boundary after the initial time. Instead of a continuous supply of particles, we accumulate the temporal sequence data of the particles during $\omega_{pi}\tau = 0$–300 in order to mimic particles continuously supplied under a steady state. Thus, when we plot the velocities of particles in **Figure 11**, we display not only the particles which are in a certain area at the instance of $\omega_{pi}\tau = 300$, but the particles which were and are in the area by $\omega_{pi}\tau = 300$. We record the particle data every $\omega_{pi}\Delta\tau = 3$, and treat an identical particle at a past time as a different particle. This means that some particles are displayed in **Figure 11** multiple times.

The fact that the test ions have initial velocities equal to the ion fluid velocity means that ions with zero temperature are hypothetically set. Consequently, we can significantly reduce the ring's width v_{width}. In **Figures 11A,B**, we plot velocities $(v_{\tilde{x}}, v_{\tilde{y}})$ of the ions inside the boxed areas (d1) and (d2) designated in **Figure 5C**, where the velocity distributions in **Figure 6** are observed. In the both cases, we can clearly see a ring-shaped structure (with an additional horn-shaped structure), which can not be seen by means of particle simulations.

On the basis of the result that in a test particle simulation run for $B_g = 1.0$, ring-shaped structures are created at the positions corresponding to **Figure 6**, we can derive a plausible interpretation as follows. In the velocity distributions shown in **Figure 6**, ring-shaped structures with a finite width surely exist, but the width is so large that they are observed as pseudo-Maxwellian distributions. Therefore, it is definitely confirmed that the velocity distributions of **Figure 6** are pseudo-Maxwellian distributions.

6 DISCUSSION AND SUGGESTION

As we described in **Section 5**, we hypothetically treat cold ions with zero temperature in the test particle simulation run, by assigning the initial velocities equal to the ion fluid velocity at each position. Nevertheless, the ring-shaped structures shown in **Figure 11** have a finite width. The fluid velocity slightly depends on the position in the upstream boundary, and ions which exist in a small area of the downstream are ones which have come from different positions in the upstream. Hence, the ions in a small area of the downstream have slightly different velocities, which contribute to the width of a ring. In addition, if some adiabatic ions, which are not responsible for the pickup-like process, exist, they will affect the shape of a velocity distribution. Furthermore, the electromagnetic field is not completely uniform in the downstream. This non-uniformity enhances variation of ion velocities. Chaotic motions of ions might play a role in producing variations of their velocities (Zenitani et al., 2017). These topics are beyond the current work, and will be discussed as a future work.

Let us suggest that pseudo-Maxwellian distributions would have been misidentified as genuine-Maxwellian distributions in particle simulations and satellite observations, since the two kinds of distributions are almost indistinguishable in shape from each other. A pseudo-Maxwellian velocity distribution is a kind of ring-shaped distribution, and it is an indicator showing that particles behave as nonadiabatic and are effectively heated through the pickup or the pickup-like process. Although effective heating events by the pickup or the pickup-like process occur in various situations more frequently or more universally than expected, they would have been overlooked so far.

Though the motivation of the present work stems from magnetic reconnection, the application of the theory of the pseudo-Maxwellian distribution will not be limited to magnetic reconnection. Let us generalize the situation as follows. Seed charged particles satisfy shifted Maxwellian distribution $\exp[-(v - v_d)^2/(2v_{T0}^2)]$, and the seed particles are continuously supplied to a region where a magnetic field $\boldsymbol{B}$ and an

electric field $\boldsymbol{E}$ are imposed. Under this generalized situation, $u_{\rm out}$ on the right-hand side of **Eq. 10** should be the relative velocity between the averaged velocity of the seed particles and the $E \times B$ drift velocity in the region. We do not need the existence of a plasma flow corresponding to the reconnection outflow, and all we need is $\boldsymbol{E}$ and $\boldsymbol{B}$ causing $E \times B$ drift motion. Based on the above arguments, we can derive the necessary condition to pseudo-Maxwellian distributions as

$$v_{T0} > \frac{1}{\sqrt{2}} \left| \frac{c\boldsymbol{E} \times \boldsymbol{B}}{B^2} - \boldsymbol{v}_{d\perp} \right|, \tag{14}$$

where $\boldsymbol{v}_{d\perp}$ is the perpendicular component of $\boldsymbol{v}_d$ to $\boldsymbol{B}$, i.e., $\boldsymbol{v}_{d\perp} = \boldsymbol{v}_d - [\boldsymbol{v}_d \cdot \boldsymbol{B}/B]\boldsymbol{B}/B$. The effective thermal velocity for the newly created velocity distribution is

$$v_{T\rm eff}^2 = \frac{1}{2} \left(\frac{c\boldsymbol{E} \times \boldsymbol{B}}{B^2} - \boldsymbol{v}_{d\perp} \right)^2 + v_{T0}^2. \tag{15}$$

7 SUMMARY

By means of theory and simulations, we have explored the feature of a ring-shaped velocity distribution with a finite width, which is newly formed as a result of the pickup-like process during magnetic reconnection in the presence of a guide magnetic field.

On the basis of a steady feeding of particles which satisfy a Maxwellian velocity distribution and a mixing of gyration phases, we have analytically derived a function which exactly expresses rings with a finite width. Moreover, the formulated function indicates that if the width is larger than $1/\sqrt{2}$ of the radius, the dip of a ring's center, i.e., the central local minimum is transformed into the peak of a mountain shape, i.e., the maximum. The mountain-like velocity distribution is almost indistinguishable in shape from a Maxwellian velocity distribution. We have named such a distribution a pseudo-Maxwellian distribution.

We have carried out particle simulations of magnetic reconnection with a guide magnetic field, and demonstrated that mountain-like velocity distributions of ions are formed in the downstream. On the basis of the existing of additional horn-shaped distributions, which is a signature showing that the pickup-like process does work, we have almost concluded that the mountain-like distributions are pseudo-Maxwellian velocity distributions. Alone by the above results, however, we could not completely disprove that they are genuine-Maxwellian, because the pseudo-Maxwellian and genuine-Maxwellian distributions are almost indistinguishable in shape from each other.

Hence, we have shown two types of evidence for pseudo-Maxwellian distributions. First, we have clarified the dependence of velocity distributions on the guide magnetic field, by performing a series of particle simulation runs. It has been found that as the guide field is larger, a ring-shaped structure with a finite width gradually becomes clearer in velocity distributions. It is because a ring's width, which is caused by velocity variations mainly due to the genuine thermal speed in the upstream, and the ring's radius, which corresponds to the reconnection outflow speed, depend on the guide field. Next, we have performed a test particle simulation, in which the motions of test ion particles with an artificial zero temperature are calculated in an electromagnetic field given by a particle simulation run. The artificial zero temperature considerably contributes to reducing the ring width. As the given field, we have employed one which has formed mountain-like velocity distributions in the particle simulation run. In the test particle simulation, we have observed clear structures of ring-shaped velocity distributions, which have not been seen in the particle simulation run. From the two types of evidence, it has been confirmed that the mountain-like velocity distributions found in the particle simulations are pseudo-Maxwellian distributions. Furthermore, the findings suggest that pseudo-Maxwellian distributions would be formed in various cases of magnetic reconnection with a guide field.

DATA AVAILABILITY STATEMENT

The raw data supporting the conclusions of this article will be made available by the authors, without undue reservation.

AUTHOR CONTRIBUTIONS

SU constructed the theory, carried out particle simulations and test particle simulations by using supercomputers, analyzed the simulation data, and wrote the paper. RH developed and improved the simulation code "PASMO," and revised the manuscript.

FUNDING

This work was supported by JSPS KAKENHI (Grant Numbers 16K17847, 15H05750, 20H00136), the General Coordinated Research at the National Institute for Fusion Science (NIFS21KNSS154), "Joint Usage/Research Center for Interdisciplinary Large-scale Information Infrastructures," and "High Performance Computing Infrastructure" in Japan (Project ID: jh210005-NAH).

ACKNOWLEDGMENTS

One of the authors (SU) appreciates advice from S. Zenitani so as to construct the theory in **Section 2**. This simulation work was performed on the supercomputers "Plasma Simulator" (NEC SX-Aurora TSUBASA) at the National Institute for Fusion Science, Japan and "Flow" (FUJITSU PRIMEHPC FX1000) at the Information Technology Center, Nagoya University, Japan.

REFERENCES

Ashour-Abdalla, M., and Kennel, C. F. (1978). Nonconvective and Convective Electron Cyclotron Harmonic Instabilities. *J. Geophys. Res.* 83, 1531–1543. doi:10.1029/JA083iA04p01531

Bessho, N., Chen, L. J., and Hesse, M. (2016). Electron Distribution Functions in the Diffusion Region of Asymmetric Magnetic Reconnection. *Geophys. Res. Lett.* 43, 1828–1836. doi:10.1002/2016GL067886

Birdsall, C. K., and Langdon, A. B. (1991). *Plasma Physics via Computer Simulation*. London: IoP Publishing Ltd.

Burch, J. L., Torbert, R. B., Phan, T. D., Chen, L.-J., Moore, T. E., Ergun, R. E., et al. (2016). Electron-scale Measurements of Magnetic Reconnection in Space. *Science* 352, aaf2939. doi:10.1126/science.aaf2939

Cheng, C. Z., Inoue, S., Ono, Y., and Horiuchi, R. (2015). Physical Processes of Driven Magnetic Reconnection in Collisionless Plasmas: Zero Guide Field Case. *Phys. Plasmas* 22, 101205. doi:10.1063/1.4932337

Drake, J. F., Cassak, P. A., Shay, M. A., Swisdak, M., and Quataert, E. (2009). A Magnetic Reconnection Mechanism for Ion Acceleration and Abundance Enhancements in Impulsive Flares. *ApJ* 700, L16–L20. doi:10.1088/0004-637X/700/1/L16

Drake, J. F., and Swisdak, M. (2014). The Onset of Ion Heating during Magnetic Reconnection with a strong Guide Field. *Phys. Plasmas* 21, 072903. doi:10.1063/1.4889871

Hesse, M., Norgren, C., Tenfjord, P., Burch, J. L., Liu, Y.-H., Chen, L.-J., et al. (2018). On the Role of Separatrix Instabilities in Heating the Reconnection Outflow Region. *Phys. Plasmas* 25, 122902. doi:10.1063/1.5054100

Horiuchi, R., and Sato, T. (1997). Particle Simulation Study of Collisionless Driven Reconnection in a Sheared Magnetic Field. *Phys. Plasmas* 4, 277–289. doi:10.1063/1.872088

Horiuchi, R., Usami, S., Moritaka, T., and Ono, Y. (2019). Particle Simulation Studies of Merging Processes of Two Spherical-tokamak-type Plasmoids. *Phys. Plasmas* 26, 092101. doi:10.1063/1.5104281

Inomoto, M., Ushiki, T., Guo, X., Sugawara, T., Kondo, K., Mihara, T., et al. (2019). Effects of Reconnection Downstream Conditions on Electron Parallel Acceleration during the Merging Start-Up of a Spherical Tokamak. *Nucl. Fusion* 59, 086040. doi:10.1088/1741-4326/ab1e0f

Ishizawa, A., and Horiuchi, R. (2005). Suppression of Hall-Term Effects by Gyroviscous Cancellation in Steady Collisionless Magnetic Reconnection. *Phys. Rev. Lett.* 95, 045003. doi:10.1103/PhysRevLett.95.045003

Mithaiwala, M., Rudakov, L., and Ganguli, G. (2010). Stability of an Ion-Ring Distribution in a Multi-Ion Component Plasma. *Phys. Plasmas* 17, 042113. doi:10.1063/1.3372842

Möbius, E., Hovestadt, D., Klecker, B., Scholer, M., Gloeckler, G., and Ipavich, F. M. (1985). Direct Observation of He+ Pick-Up Ions of Interstellar Origin in the Solar Wind. *Nature* 318, 426–429. doi:10.1038/318426a0

Ohtani, H., and Horiuchi, R. (2009). Open Boundary Condition for Particle Simulation in Magnetic Reconnection Research. *Plasma Fusion Res.* 4, 024. doi:10.1585/pfr.4.024

Ono, Y., Inoue, S., Tanabe, H., Cheng, C. Z., Hara, H., and Horiuchi, R. (2019). Reconnection Heating Experiments and Simulations for Torus Plasma Merging Start-Up. *Nucl. Fusion* 59, 076025. doi:10.1088/1741-4326/ab14a4

Pei, W., Horiuchi, R., and Sato, T. (2001). Ion Dynamics in Steady Collisionless Driven Reconnection. *Phys. Rev. Lett.* 87, 235003. doi:10.1103/PhysRevLett.87.235003

Pei, W., Horiuchi, R., and Sato, T. (2001). Long Time Scale Evolution of Collisionless Driven Reconnection in a Two-Dimensional Open System. *Phys. Plasmas* 8, 3251–3257. doi:10.1063/1.1375150

Pucci, F., Usami, S., Ji, H., Guo, X., Horiuchi, R., Okamura, S., et al. (2018). Energy Transfer and Electron Energization in Collisionless Magnetic Reconnection for Different Guide-Field Intensities. *Phys. Plasmas* 25, 122111. doi:10.1063/1.5050992

Tanabe, H., Tanaka, H., Cao, Q., Cai, Y., Akimitsu, M., Ahmadi, T., et al. (2021). Global Ion Heating/transport during Merging Spherical Tokamak Formation. *Nucl. Fusion* 61, 106027. doi:10.1088/1741-4326/ac217c

Tanabe, H., Yamada, T., Watanabe, T., Gi, K., Inomoto, M., Imazawa, R., et al.The MAST Team (2017). Investigation of Merging/reconnection Heating during Solenoid-free Startup of Plasmas in the MAST Spherical Tokamak. *Nucl. Fusion* 57, 056037. doi:10.1088/1741-4326/aa6608

Thorne, R. M., and Summers, D. (1989). Kinetic Instability of a Gyrating Ring Distribution with Application to Satellite Pickup in Planetary Magnetospheres. *Planet. Space Sci.* 37, 535–544. doi:10.1016/0032-0633(89)90094-9

Usami, S., Horiuchi, R., and Ohtani, H. (2017). Effective Heating of Nonadiabatic Protons in Magnetic Reconnection with a Guide Field. *Phys. Plasmas* 24, 092101. doi:10.1063/1.4997453

Usami, S., Horiuchi, R., and Ohtani, H. (2019). Horn-Shaped Structure Attached to the Ring-Shaped Ion Velocity Distribution during Magnetic Reconnection with a Guide Field. *Plasma Fusion Res.* 14, 3401137. doi:10.1585/pfr.14.3401137

Usami, S., Horiuchi, R., Ohtani, H., Ono, Y., Inomoto, M., and Tanabe, H. (2019). Dependence of the Pickup-like Ion Effective Heating on the Poloidal and Toroidal Magnetic fields during Magnetic Reconnection. *Phys. Plasmas* 26, 102103. doi:10.1063/1.5099423

Winske, D., and Daughton, W. (2012). Generation of Lower Hybrid and Whistler Waves by an Ion Velocity Ring Distribution. *Phys. Plasmas* 19, 072109. doi:10.1063/1.4736983

Wu, C. S., and Davidson, R. C. (1972). Electromagnetic Instabilities Produced by Neutral-Particle Ionization in Interplanetary Space. *J. Geophys. Res.* 77, 5399–5406. doi:10.1029/JA077i028p05399

Wu, C. S., Yoon, P. H., and Freund, H. P. (1989). A Theory of Electron Cyclotron Waves Generated along Auroral Field Lines Observed by Ground Facilities. *Geophys. Res. Lett.* 16, 1461–1464. doi:10.1029/GL016i012p01461

Yamada, M. (2007). Progress in Understanding Magnetic Reconnection in Laboratory and Space Astrophysical Plasmas. *Phys. Plasmas* 14, 058102. doi:10.1063/1.2740595

Yamada, M., Yoo, J., Jara-Almonte, J., Ji, H., Kulsrud, R. M., and Myers, C. E. (2014). Conversion of Magnetic Energy in the Magnetic Reconnection Layer of a Laboratory Plasma. *Nat. Commun.* 5, 4774. doi:10.1038/ncomms5774

Yoon, Y. D., and Bellan, P. M. (2021). How Hall Electric fields Intrinsically Chaotize and Heat Ions during Collisionless Magnetic Reconnection. *Phys. Plasmas* 28, 022113. doi:10.1063/5.0040374

Zenitani, S., Hasegawa, H., and Nagai, T. (2017). Electron Dynamics Surrounding the X Line in Asymmetric Magnetic Reconnection. *J. Geophys. Res. Space Phys.* 122, 7396–7413. doi:10.1002/2017JA023969

Zenitani, S., and Nagai, T. (2016). Particle Dynamics in the Electron Current Layer in Collisionless Magnetic Reconnection. *Phys. Plasmas* 23, 102102. doi:10.1063/1.4963008

Conflict of Interest: The authors declare that the research was conducted in the absence of any commercial or financial relationships that could be construed as a potential conflict of interest.

Publisher's Note: All claims expressed in this article are solely those of the authors and do not necessarily represent those of their affiliated organizations, or those of the publisher, the editors, and the reviewers. Any product that may be evaluated in this article, or claim that may be made by its manufacturer, is not guaranteed or endorsed by the publisher.

Copyright © 2022 Usami and Horiuchi. This is an open-access article distributed under the terms of the Creative Commons Attribution License (CC BY). The use, distribution or reproduction in other forums is permitted, provided the original author(s) and the copyright owner(s) are credited and that the original publication in this journal is cited, in accordance with accepted academic practice. No use, distribution or reproduction is permitted which does not comply with these terms.